# Investigation of Mechanical, Corrosion and Microstructural Behaviour of Heat Treated Cr-Modified Al-Mg-Si Alloy

## Olusegun Olufemi Ajide [a], Temilade Ruth Adelakun [a], Itopa Godwin Akande [b*], Temilola Taiwo Olugasa [a] and Nikhil Kumar [c]

[a] *Department of Mechanical Engineering, University of Ibadan, Ibadan, Oyo State, Nigeria.*
[b] *Department of Automotive Engineering, University of Ibadan, Ibadan, Oyo State, Nigeria.*
[c] *School of Materials Science and Technology, Indian Institute of Technology (BHU), Varanasi-221005, India.*

*Authors' contributions*

*This work was carried out in collaboration among all authors. Author OOA did the research conceptualization, designed the methodology, supervision of the experimentations, reviewed and updated the first draft of the manuscript. Author TRA performed the experiments, characterizations and wrote the first draft of the manuscript. Author IGA performed corrosion analysis and interpretation of microstructures data. In addition, author IGA reviewed and co-wrote the updated version of the manuscript. Author TTO co-supervise the research and edited the manuscript. Author NK co-interpreted the microstructures data and edited the manuscript. All authors jointly responded to the reviewers' comments, read and approved the final manuscript.*

*Original Research Article*

## ABSTRACT

Despite the choice of Al-Mg-Si alloy as a material for innumerable industrial and structural applications, challenges such as undesired scratch resistance, formability and mechanical properties deterioration in saline environment hinders the extent of its application for automotive

and aerospace components. Nevertheless, with the growing interest in the application of Al-Mg-Si alloy in automotive and aerospace industries, there is need for cautious control of thermal treatments and inclusion of alloying elements with requisite potentials for enhancing the microstructure and mechanical properties of the alloy. Chromium is known to improve strength and corrosion resistance in several applications. Therefore, this study focuses on the investigation of the effect of Cr particles inclusion in Al-Mg-Si alloy. The effect of ageing heat treatment on selected properties of Al-Mg-Si-Cr alloy was also studied in this work. The Al-Mg-Si and Al-Mg-Si-Cr alloys were developed using a two-step stir casting technique. Chromium was added to Al-Mg-Si alloy at varying percentages of 0, 0.5, 1.0, 1.5, 2.0 and 2.5. All the samples were solution treated in an electric furnace at 500 $^{o}$C for 30 minutes and water quenched. Then the samples were artificially aged at 210 $^{o}$C for 3 hours and quenched in natural air. The hardness test revealed that the inclusion of Cr particles in Al-Mg-Si alloy samples increased hardness from 35.03 Kgf/mm$^2$ (hardness of Al-Mg-Si-0%Cr alloy sample) to a maximum value of 126.54 Kgf/mm$^2$ (hardness of Al-Mg-Si-1.5%Cr alloy sample). After heat treatment, the hardness of Al-Mg-Si-0%Cr alloy sample increased to 80.84 Kgf/mm$^2$, while that of Al-Mg-Si-1.5%Cr alloy sample decreased slightly to 120.88 Kgf/mm$^2$. The impact strength test also showed that the inclusion of Cr in Al-Mg-Si alloy increased impact strength from 9.52 J/mm$^2$ (impact strength of Al-Mg-Si-0%Cr alloy sample) to a maximum value of 19.04 J/mm$^2$ (impact strength of Al-Mg-Si-2.0%Cr alloy sample). After heat treatment, the impact strength of Al-Mg-Si-0%Cr alloy sample increased marginally to 10.09 J/mm$^2$, while that of Al-Mg-Si-2.0%Cr alloy sample decreased slightly to 17.57 J/mm$^2$. The tensile and electrochemical tests revealed that the heat-treated Al-Mg-Si-1.0%Cr alloy sample exhibited the highest tensile strength and lowest corrosion rate of 152 MPa and 0.0014 mm/year, respectively. The microstructural examination further revealed that the inclusion of Cr particles in Al-Mg-Si alloy improved its surface morphology. Al-Mg-Si-1.0%Cr alloy sample was adjudged to possess the best microstructural properties. Therefore, this sample is recommended as a potential material for machine tools and other structural or advanced manufacturing applications.

## ABBREVIATIONS

*SEM*     *: Scanning electron microscope*
*ASTM*    *: American society for testing and materials*
*CR*        *: Corrosion rate*
*OCP*     *: Open circuit potential*
*$j_{corr}$*     *: Corrosion current density*
*Rp*       *: Polarization resistance*
*$E_{corr}$*    *: Corrosion potential*

## 1. INTRODUCTION

Aluminium alloys are widely used in the automotive industry as an alternative material to steel. The attraction for Al alloys is due to their low density, recyclability, superior mechanical properties and good corrosion resistance [1-3]. The corrosion resistance property of Al alloys is as a result of the stability of the aluminium oxide layer formation on exposure to air [4-6]. Material designers have also shifted emphasis to the pursuit of low cost and high-performance characteristics materials like Al alloys, which are suitable for the products required [7,8]. The scope of these materials is further expanded with the help of post-processing treatment and alloying elements, which combines the individual properties of those materials to create the desired products properties [9,10]. Post-processing treatments such as heat treatment have played major roles in recent developments in this field since it promotes a general refinement of the microstructure and improves the physical properties of alloys [11-13]. Heat-treatment has also been reported to improve the strength of aluminium alloys through a process known as precipitation-hardening which occurs during the heating and cooling of the alloy, with the formation of precipitates matrix of the alloy [14-16]. Likewise, ageing heat treatment has been used for the improvement of the microstructure of aluminium alloys. Two different methods of ageing: artificial and natural ageing have been reported in many works of literature [17-19].

Moreso, microstructure and other properties of aluminium alloys have been improved through the addition of alloying elements such as Si, Mn, Cr, Cu, Zn, Sn, Ag, Fe, e.t.c [20-22]. For instance, some of these alloying elements have been included in Al-Mg-Si alloys by a good

number of researchers to produce a selection of different materials that can be used in a wide assortment of structural applications [23-26]. Chromium was discovered to increase the low-temperature properties and enhanced the creep resistance of Al-Mg-Si alloys marginally [27,28]. The study also revealed that Mn and Cr additions affect the kinetics of recrystallization and parameters of grain-boundary relaxation of Al-4.9Mg alloys. The Cr particles helps in preventing recrystallization and grain growth, hence refining the grains [29]. Chromium has been used as alloy addition to AA6xxx alloys to control the grain structure by producing dispersoids that pin grains and limit grain growth. Thus, the mechanical properties of the aluminium alloys were improved [30]. Grain refinement plays a vital function in determining the significant characteristics of aluminium alloy products. It enhances plasticity and tensile intensities, increases feeding complex castings, and minimizes the possibility of hot tearing and porosity [31,32].

Furthermore, chromium is a common addition to many alloys of the aluminium–magnesium series because it has a large effect on electrical resistivity. Chromium has a low diffusion rate and forms finely dispersed phases in wrought products. Extensive literature studies indicate that major work has been carried out on Al-Mg-Si-Cr alloy for many structural applications. The need to improve the properties and quality of aluminium alloy using simple foundry and conventional casting technique for the economic development of aluminium alloy instigates the need for this work. Al-Mg-Si alloy has been widely used for several industrial and structural applications [33-36]. However, due to a few challenges, it is rarely used for some advanced structural applications. The main aim of this work is to examine the effect of chromium addition on the mechanical, microstructural and corrosion properties of Al-Mg-Si alloy. This work further examined the effect of heat treatment on the mechanical, microstructural and corrosion characteristics of Al-Mg-Si-Cr alloys. Heat-treating the alloys containing the appropriate percentage of Cr particles was done and examined for potential machine tools applications.

## 2. MATERIALS AND METHODS

### 2.1 Alloy Production

Aluminium scrap (mostly trophy beverage cans) was sourced and used as the base aluminium alloy. This decision was made to show that aluminium waste in our environment can be converted into a very good choice material for different kinds of engineering applications. Using optical emission spectroscopy, the approximate chemical compositions of the alloy are: 1.50% manganese (Mn), 0.70% iron (Fe), 0.20% copper (Cu), 0.05% magnesium (Mg), 0.60% silicon (Si), 0.10% zinc (Zn) and Al balance as the principal element. This characterization revealed that the alloy is Al 3003 alloy. These are similar to those of authors Ref. [37]. The volume percentage by weight of magnesium and silicon was constant at 0.6% and 7%, respectively for all the samples. The mass of Al 3003 alloy was also constant at 500 g for all the samples. The chemical composition of the experimental alloys is shown in Table 1, which indicated that chromium was incorporated into Al-Mg-Si composite at levels of 0, 0.5,1, 1.5, 2 and 2.5% using the two-step stir casting method (liquid metallurgy technique) to produce Al-Mg-Si-Cr alloy. The Aluminum 3005 alloys having 92.4, 91.9, 91.4, 90.9, 90.4, and 89.9 percent by weight, based on the charge calculations, were at first heated to 300 $^o$C for 45 minutes to aid the alloy's wettability. The magnesium and chromium powder were preheated to 900$^o$C and silicon particles were also preheated to 1100$^o$C to further aid the alloy's wettability. Thereafter, the Al 3003 alloy particles were charged into a furnace at 780$^o$C, and allowed to dispel heat until the alloy was in a semi-solid form at about 600$^o$C. At the semi-solid stage of the Al 3003 alloy, preheated magnesium, silicon and chromium powder were introduced into the alloy, and manually stirred for 5-7 minutes.

### 2.2 Heat Treatment

The cast products of Al-Mg-Si and Al-Mg-Si-Cr alloys were made to undergo heat treatment. The heat treatment was carried in an electric furnace. All the samples were solution heat treated in an electric furnace at 500$^o$C for 30 minutes and were water quenched after which they were aged. T6 condition was applied to products that are solution heat-treated and then aged artificially. All the samples were aged artificially at 210$^o$C for 3 hours and then quenched in natural air.

### 2.3 Electrochemical Test

A computer-controlled potentiostat, NOVA 2.1 was used for the electrochemical study. The analysis was performed using NOVA 2.1 electrochemical software and a three-electrode

corrosion cell set up containing a counter electrode (CE), reference electrode (RE) and alloys as the working electrode (WE). The samples for the polarization test (WE) were cut out into 10 mm x10 mm and mounted on epoxy resin. The exposed surfaces of the samples were prepared by polishing them with emery cloths with increasing grit size from 60–1200. Afterwards, the CE, RE and the WE were connected, and thereafter inserted in an electrolyte (3.5 wt.% NaCl). Exposed surfaces area of 100 mm$^2$ was ensured for the samples in the electrolyte. Time was allowed for the samples to reach open circuit potential (OCP) in the test medium and was noted. Polarization was measured at a scan rate of 1mV/s at a potential initiated at −250 mV to +250 mV. The Tafel curves were plotted; the anodic and cathodic polarization curves of the Tafel were further extrapolated to obtain the values of corrosion current densities (jcorr) and corrosion potentials. The corresponding corrosion rates (CR) for the alloys were then determined using Equation 1 [38].

$$\text{CR (mm/yr)} = \frac{0.00327 \text{x EW x j}_{corr}}{\rho} \qquad (1)$$

Where: jcorr (A/cm$^2$) is the corrosion current density, EW (g) is the equivalent weight of the metal and ρ (g/cm$^3$) is the density of the metal.

## 2.4 Mechanical Tests

### 2.4.1 Brinell's hardness

Brinell's hardness test was used to determine the hardness of the metal surfaces. The hardness test was carried out following ASTM A29/A29M-15. For this test, the specimens of Al-Mg-Si and Al-Mg-Si-Cr alloys were cut to cylindrical shapes of length 30mm and diameter 8mm. The specimens were polished to remove the possible presence of defects. The specimens were then placed under a standard steel ball (indenter) of diameter 10 mm and the mercury gauge was set

to zero as the reference point on the tester. The force of 225 kgf as indicated on the mercury gauge was applied on the specimens for about 15 seconds. The indentation diameters on the specimens were measured after the load and ball were removed. The Brinell hardness numbers of the samples were then calculated using Equation 2 [39].

$$\text{BHN} = \frac{2F}{\pi d[(d - \sqrt{(d^2 - D^2)}]} \qquad (2)$$

Where D and d are the diameter of indentations and diameter of the steel ball, respectively, while F is the applied force.

### 2.4.2 Tensile strength

Tensometer was used to carry out the tensile strength test. The specimens were machined, thereafter shaped into standard test piece size; cylindrical shape of length 30 mm and diameter 5 mm with dog bone-shaped ends. The initial diameter ($d_0$) and length ($L_0$) of the specimen were observed before the start of the test. One end of the specimen was fastened to the frame of the machine using grips, while the other end was similarly fixed to the movable crosshead. A steadily increasing load was applied to the specimen by pulling the hand wheel of the machine in a clockwise direction. The magnitude of the load was measured by the pointer on the load measuring unit. The yield point was measured on the pointer when the mercury stopped moving in the forward direction for a short while. On the further increase of the load, the pointer got to the ultimate load and at that point, the pointer moved in the reverse direction and stopped at a point to cause a fracture of the specimen. Thereafter, the fractured specimens were arranged together and the final length ($L_f$) and diameter ($d_f$) of each specimen were measured. Then, the computation of average tensile strength values was done following ASTM E8 standard.

**Table 1. Chemical composition of the experimental alloys**

| Sample | Percentage of Al 3003 (%) | Weight of Mg (g) | Weight of Si (g) | Percentage of Cr (%) | Weight of Cr (g) |
|---|---|---|---|---|---|
| Al-Mg-Si-0%Cr | 92.4 | 3.25 | 37.88 | 0 | 0 |
| Al-Mg-Si-0.5%Cr | 91.9 | 3.26 | 38.08 | 0.5 | 2.72 |
| Al-Mg-Si-1.0%Cr | 91.4 | 3.28 | 38.29 | 1.0 | 5.47 |
| Al-Mg-Si-1.5%Cr | 90.9 | 3.30 | 38.5 | 1.5 | 8.25 |
| Al-Mg-Si-2.0%Cr | 90.4 | 3.32 | 38.72 | 2.0 | 11.06 |
| Al-Mg-Si-2.5%Cr | 89.9 | 3.34 | 38.93 | 2.5 | 13.9 |

### 2.4.3 Impact strength

Impact strength (IS) is the ability of materials to absorb shock energy before the occurrence of deformation or fracture. The IS of the various alloy samples was examined via pendulum-type IS testing machine following ASTM D256. Each specimen was cut to the diameter of 10 mm and a length of 120 mm. This was followed by the notching of a 2 mm groove on the specimens for effective fitting into the machine. The specimens were mounted on the machine, allowing the pendulum to fall from a fixed point of a known height to deform or fracture the specimen. The impact strength is then indicated by the pointer on the scale after the occurrence of fracture.

## 2.5 Microstructural Examination

The specimens were grinded, polished and etched. Silicon carbide papers of different grades (220, 320, 400 and 600) were positioned on the grinding machine. A selvt cloth (polishing cloth) was swamped with 1.0 micron of silicon carbide solution. Ultimate polishing was carried out by swamping the polishing cloth with silicon carbide of 0.5 microns until a mirror-like surface was achieved. The mirror-like surface was etched in 2% sodium hydroxide solution for 45 seconds. The samples were thereafter subjected to microstructural examination using an optical microscope (OPM) and scanning electron microscope (SEM) at the magnification of 400× and 250×, respectively.

## 3. RESULTS AND DISCUSSION

### 3.1 Electrochemical Properties

The polarization curves (Tafel curves) and polarization data for Al-Mg-Si and Al-Mg-Si-Cr alloy samples in 3.5 wt.% NaCl medium are shown in Fig. 1 and Table 2, respectively. Compared to other samples, the Al-Mg-Si alloy sample containing 0% Cr particles exhibited the highest corrosion rate and peak corrosion current density (jcorr) of 47.4840 mm/year and 4.10 E-03 A/cm$^2$, respectively. These values indicated that the corrosive medium ingresses the anodic and cathodic sites of the alloy to a greater extent compared to other samples. Also, the lowest polarization resistance (Rp) exhibited by the sample suggests that the medium was more active in the presence of Al-Mg-Si-%Cr alloy sample compared to each of the Al-Mg-Si-Cr alloy samples, leading to a high corrosion rate. Generally, all the Al-Mg-Si-Cr alloy samples exhibited significantly low corrosion rate and corrosion current density in 3.5% NaCl medium compared to Al-Mg-Si-%Cr alloy sample, indicating that the chromium particles inclusion into the matrix of Al-Mg-Si alloy was able to fill some micro holes, thereby minimizing the penetration of corrosive products and ions from 3.5% NaCl medium. The low values of the corrosion current densities also implied that the particles of Cr minimized the exchange of current between the anodic and cathodic sites of the alloys [40,41].
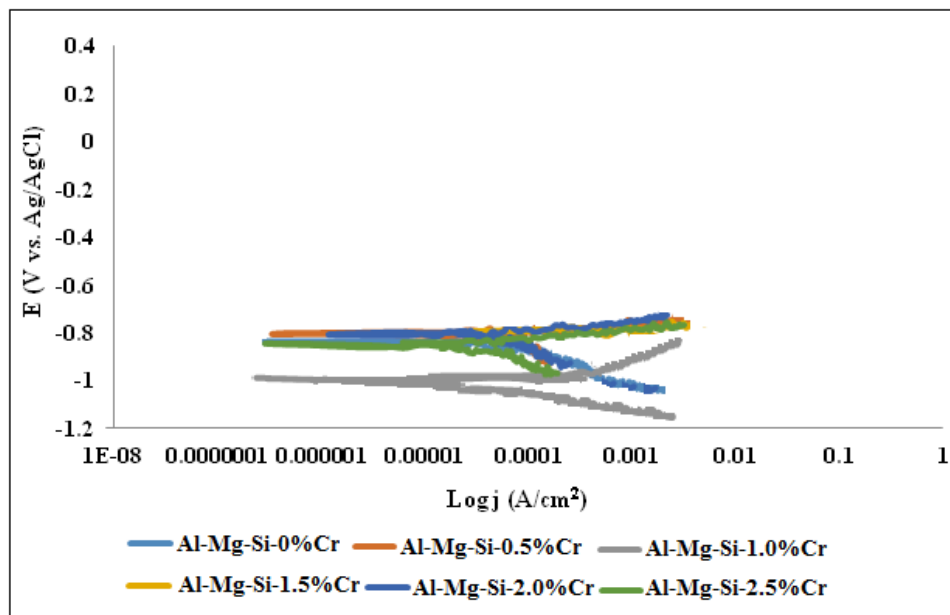


**Fig. 1. Tafel curves for Al-Mg-Si and Al-Mg-Si-Cr alloy samples in 3.5% NaCl medium**

It is also worth mentioning that Al-Mg-Si-1.0%Cr alloy sample possessed the lowest CR of 0.0014 mm/year, lowest jcorr of 1.19E-07 $A/cm^2$ and highest Rp of 9568.20 Ω. These values are good indications that minimal reaction occurs between the active sites of the alloy, perhaps due to the optimal inclusion of chromium. Fig. 1 also revealed that Cr particles tend to have a predominantly mixed corrosion protection effect on the alloy samples in 3.5% NaCl medium [42, 43]. This implied that Cr particles somewhat had a balanced corrosion protection effect on the anodic and the cathodic sites of these alloys. However, with the Al-Mg-Si-1.0%Cr alloy sample (1.0% Cr particles addition sample), the polarization curves shifted marginally towards the cathodic region of the control sample (Al-Mg-Si-0%Cr alloy sample). This indicated that Cr particles had more cathodic corrosion protection effect on this sample in the test medium (44).

Furthermore, the open circuit potential (OCP) graph, which is also referred to as the steady-state potential graph is shown in Fig. 2.

This revealed the stability of the alloys in the corrosive medium within the test period. The starting potentials for the alloy samples ranges approximately between -0.8 and -1.12 V. However, the end potentials fall approximately between -0.8 and -1.0 V due to the shift in potential by some of the samples. For instance, the Al-Mg-Si-0%Cr alloy sample started with the potential of about 1.02 V, shifted to the less negative potentials and become stable between the last 60 and 70 minutes. Similarly, the OCP of Al-Mg-Si-1.0%Cr alloy sample (1.0% Cr particles inclusion sample) was stable between the first 30 minutes of the experiment, experienced change in potentials, but eventually, become relatively stable. Moreso, a similar trend was observed with the Al-Mg-Si-1.0%Cr alloy sample. Contrary to the other samples, the samples containing Al-Mg-Si-2.0%Cr and Al-Mg-Si-2.5%Cr alloy samples exhibited stable potential throughout the experiment. In general, the behaviour of these alloys signified that stead-state potential was achieved during the period of the experiment [45,46].

**Table 2. Polarization data for Al-Mg-Si and Al-Mg-Si-Cr alloy samples in 3.5% NaCl medium**

| Sample | Ecorr (V) | Jcorr ($A/cm^2$) | CR (mm/year) | Rp (Ω) |
|---|---|---|---|---|
| Al-Mg-Si-0%Cr | -0.79583 | 4.10 E-03 | 47.4840 | 9.6567 |
| Al-Mg-Si-0.5%Cr | -0.80571 | 3.06E-05 | 0.3551 | 144.43 |
| Al-Mg-Si-1.0%Cr | -1.02530 | 1.19E-07 | 0.0014 | 9568.20 |
| Al-Mg-Si-1.5%Cr | -0.84284 | 9.91E-05 | 1.1521 | 349.63 |
| Al-Mg-Si-2.0%Cr | -0.80706 | 8.73E-05 | 1.0145 | 280.47 |
| Al-Mg-Si-2.5%Cr | -0.85355 | 4.77E-06 | 0.0554 | 562.22 |
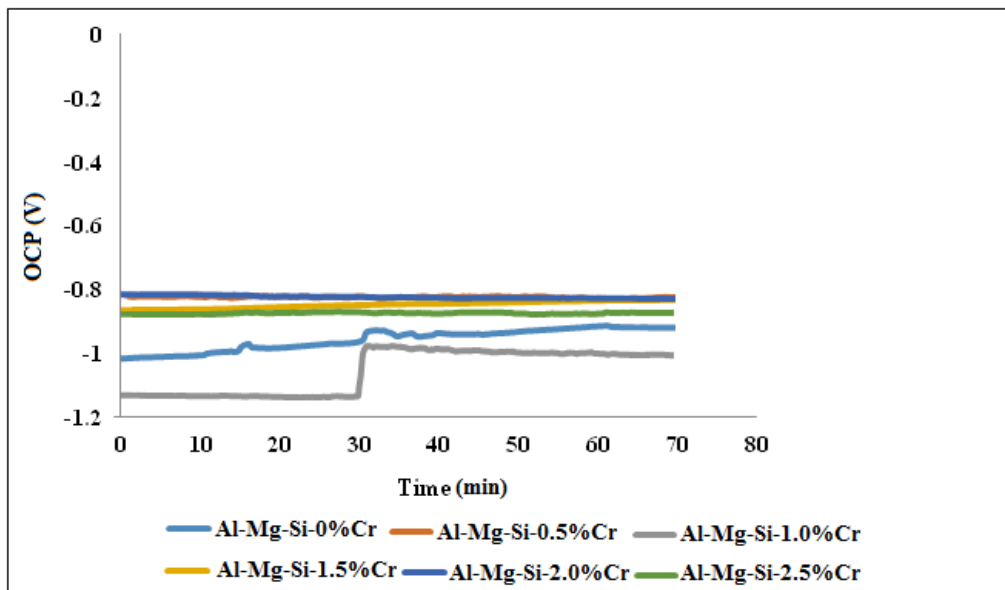


**Fig. 2. OCP for Al-Mg-Si and Al-Mg-Si-Cr alloy samples in 3.5% NaCl medium**

## 3.2 Hardness Properties

The effect of chromium inclusion and heat treatment on the Brinell's hardness of Al-Mg-Si and Al-Mg-Si-Cr alloy samples is shown in Fig. 3. The Fig. 3 showed that Al-Mg-Si alloy sample with 0% Cr particles exhibited a reasonable increase in hardness after heat treatment. There was also an increment in the hardness value of Al-Mg-Si alloy sample on the inclusion of 0.5% Cr particles. More increment in hardness value was observed on the addition of 1.0% Cr particles. An upsurge in these hardness values occurs after heat treatment. For instance, for 0.5% Cr particles addition, the hardness value increased from 56.02 $Kgf/mm^2$ to 86.73 $Kgf/mm^2$ while that of 1.0% Cr particles addition increased from 61.80 $Kgf/mm^2$ to 89.62 $Kgf/mm^2$. This could be attributed to the precipitation hardening effect of the heat treatment processes and the strengthening mechanism of chromium which can affect the hardness of the material [47-50]. A conclusion can therefore be drawn that heat treatment and increase in the percentage concentration of Cr particles resulted in the increase of hardness value of Al-Mg-Si-Cr alloy samples between 0% and 1.0% Cr particles inclusion. This behaviour justified the assertion that ageing heat treatment process promotes hardness due to the precipitates of alloying elements that hinder the movement of the dislocations [51,52]. Comparing the hardness values of all the alloy samples, the maximum

hardness value of 126.54 $Kgf/mm^2$, which reduced to 120.88 $Kgf/mm^2$ after heat treatment, was recorded for 1.50% Cr particles inclusion. This reduction could be as a result of void coalesces within the test region of the heat-treated sample [53-55]. Although, for 2.0% Cr particles inclusion, the hardness of the heat-treated Al-Mg-Si-Cr alloy sample was found to be slightly higher than the un-heat treated. Although reverse was the case for the 2.5% Cr particles inclusion. Conclusively, among the test samples, heat-treated and un-heat treated Al-Mg-Si-Cr alloy sample with 1.5% Cr particles exhibited a superior hardness characteristic, and next to it is the 2.5% Cr particles inclusion sample.

## 3.3 Impact Strength

Fig. 4 shows the effect of chromium inclusion and heat treatment on the impact strength of Al-Mg-Si and Al-Mg-Si-Cr alloy samples. It can be seen that the inclusion of 0.5% Cr particles to Al-Mg-Si alloy increased the impact strength from 9.52 $J/mm^2$ to 14.28 $J/mm^2$. However, there was a drastic reduction in impact strength to 6.12 $J/mm^2$ with 1.0 % Cr particles addition, which increased slightly to 6.39 $J/mm^2$ with 1.5 % Cr addition. The maximum impact strength of 19.04 $J/mm^2$ was obtained with 2.0% Cr particles inclusion. The value of impact strength drastically reduced to 8.16 $J/mm^2$ with the inclusion of 2.5% Cr particles. This indicated that Al-Mg-Si-Cr alloy sample with 2.0% Cr particles inclusion was able
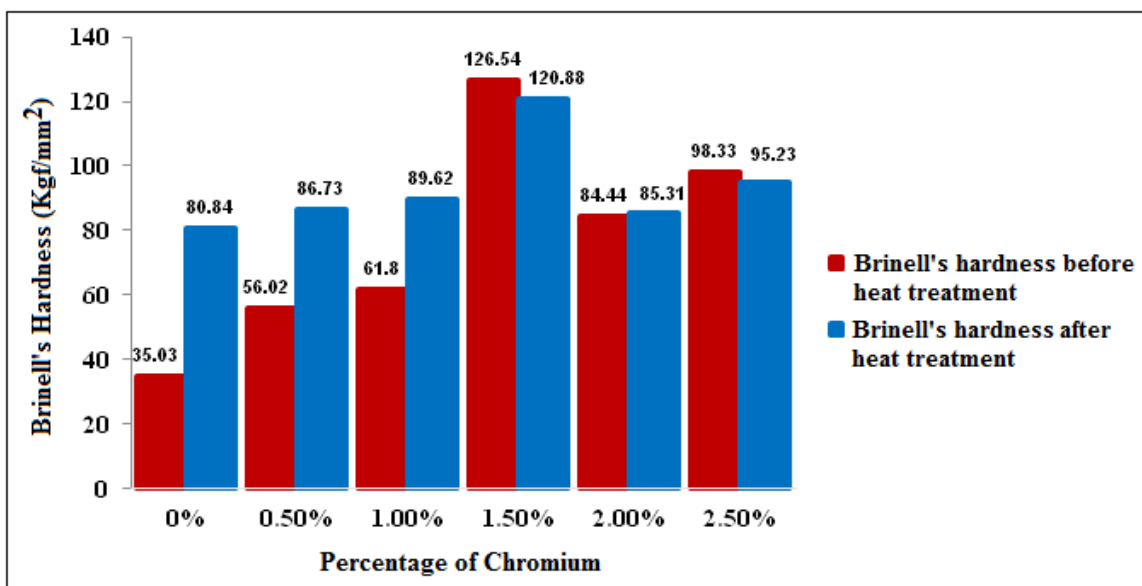


**Fig. 3. Effect of chromium and heat treatment on the Brinell's hardness of Al-Mg-Si and Al-Mg-Si-Cr alloy samples**

to absorb more shock energy before deformation or fracture. This could be ascribed to the Cr aggregation and slight load transfer between the matrix and Cr particles [56]. Other authors have also attributed this to the improved load-carrying capacity and the increased deformability of the alloy [57,58]. It can also be observed in Fig. 4 that the effect of heat-treatment is not consistent. For instance, heat treating Al-Mg-Si-Cr alloy samples with 0.5%, 2.0% and 2.5% Cr particles inclusion resulted in the reduction in their impact strength. However, this effect is not the same with 0%, 1.0% and 1.5% Cr particles inclusion, where increase in impact strength was observed after heat treatment. This indicated that these three materials can be heat treated for specific applications while others might just be used without being heat treated.

## 3.4 Ultimate Tensile Strength (UTS)

The ultimate tensile strength of heat-treated Al-Mg-Si and Al-Mg-Si-Cr alloy samples is shown in Fig. 5. The addition of 0.5% Cr particles increased the UTS from 112.02 MPa to 136.54 MPa. It further increased to 152 MPa with 1.0% Cr particles inclusion, which is the maximum UTS recorded among the test samples. This

increment in the UTS values could be ascribed to the ability of Cr particles to reduce plastic deformation on the matrix of Al-Mg-Si alloy [59, 60], and this indicated that this alloy sample offered the largest restrain to peripheral pulling, compared to other samples [61,62]. The reason for the large decrease in the UTS on the addition of 1.5% Cr particles to Al-Mg-Si alloy could be due to defects in the test region. However, significant increment in UTS was observed with 2.0% Cr particles inclusion into the matrix of Al-Mg-Si alloy. The 2.5% Cr particles inclusion in Al-Mg-Si alloy produced a highly negative effect on the alloy. Comparing the 152 MPa (UTS of Al-Mg-Si alloy sample with 1.0% Cr particles inclusion) to 67.3 MPa (UTS of Al-Mg-Si alloy sample with 2.5% Cr particles inclusion) revealed a decrement of about 125.85% in UTS value. Balasubramanian and Maheswaran [63], attributed such occurrence to the phenomenon that results in a possible reduction in the ductility of composite in micro level locality near the Cr particles and the likely presence of defects in the test region. This indicated that Al-Mg-Si alloy material with 2.5% Cr particles inclusion might not be able to withstand reasonable application load. Compared to other alloy samples, it could be more susceptible to brittle failure [64].
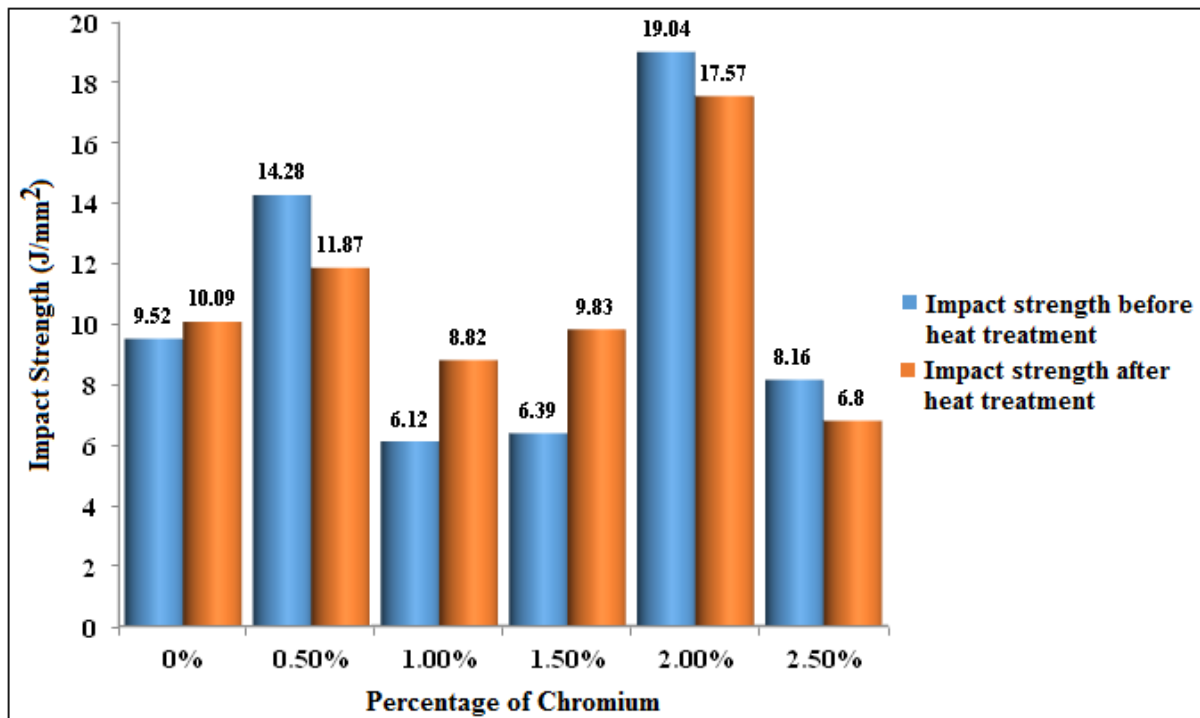


**Fig. 4. Effect of chromium and heat treatment on the impact strength of Al-Mg-Si and Al-Mg-Si-Cr alloy samples**
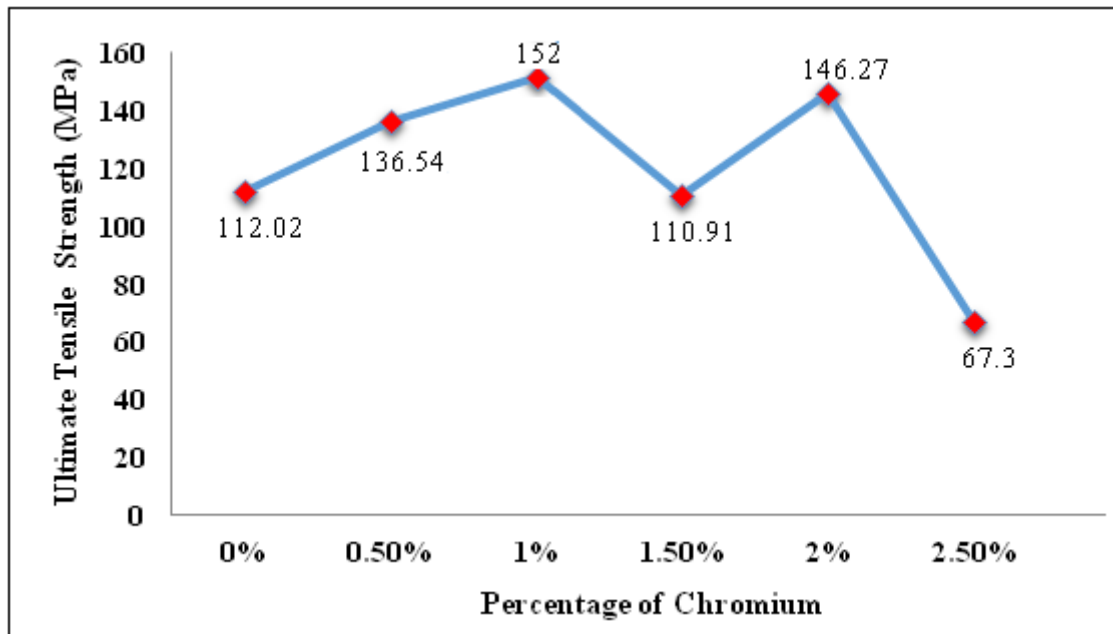
**Fig. 5. Effect of Cr and heat treatment on the ultimate tensile strength of Al-Mg-Si and Al-Mg-Si-Cr alloy samples**

## 3.5 Microstructural Properties Study of Al-Mg-Si and Al-Mg-Si-Cr Alloy Samples

Fig. 6 shows the OPM of Al-Mg-Si and Al-Mg-Si-Cr alloy samples. In Fig. 6a, more coarse and irregular morphologies were observed in the matrix of Al-Mg-Si-1.0%Cr alloy sample. Series of needle-like inhomogeneous microstructures was also noticed. This could have been the reason for the high corrosion rate of the sample. The irregular and needle-like surface morphologies could have easily acted as pitting corrosion initiation sites [65,66]. On the other hand, Fig. 6b, which is the OPM of the un-heat treated Al-Mg-Si-1.0%Cr alloy sample, exhibited more improved morphologies, with minimal macro-segregation of particles. The homogenous microstructure could be ascribed to the inclusion of Cr particles, which fill the needle-like voids visible in the matrix of Al-Mg-Si alloy. The OPM of the heat-treated Al-Mg-Si-1.0%Cr alloy sample in Fig. 6c revealed complex multiphase structure. There is also an obvious formation of fine chromium precipitates in the matrix of the alloy, resulting in a fine dispersion of the chromium-rich phases. However, the addition of 1.5% Cr particles to the matrix of Al-Mg-Si alloy resulted in the agglomeration of particles and rougher morphologies, as shown in Fig. 6d. The agglomerated particles form clusters, indicating

that the volume concentration of Cr particles could have oversaturated the matrix of Al-Mg-Si alloy [67,68]. Although, the agglomeration of the particles was found not too visible after heat treatment, as indicated in Fig. 6e. These clusters of chromium are likely to be responsible for the high hardness value of Al-Mg-Si-1.5%Cr alloy sample.

A further study carried out on Al-Mg-Si and Al-Mg-Si-Cr alloy samples using SEM is shown in Fig. 7. This was done to ascertain the effect of chromium on their microstructural properties. The presence of the reinforcing chromium powder particles was evident in the un-heat treated Al-Mg-Si-1.0%Cr and heat-treated Al-Mg-Si-1.0%Cr samples as shown in Fig. 7b and 7c, respectively. These micrographs showed that the reinforcing Cr particles and the other constituents were relatively dispersed homogenously with low agglomeration in the matrix of the alloy.

Comparing the SEM in Figs. 7b and 7c to that of Fig. 7a, it obvious that the addition of Cr particles to the matrix of Al-Mg-Si reduces the grain size of the matrix. For a nanocomposite material, the matrix grain size is dependent on the particles size and fraction. Therefore, it is observed that the Cr particles addition to the matrix of the alloy decreases the grain size, and this indicated that grain refinement occurred. The grain refinement or reduced grain size seen in Figs. 7b and 7c
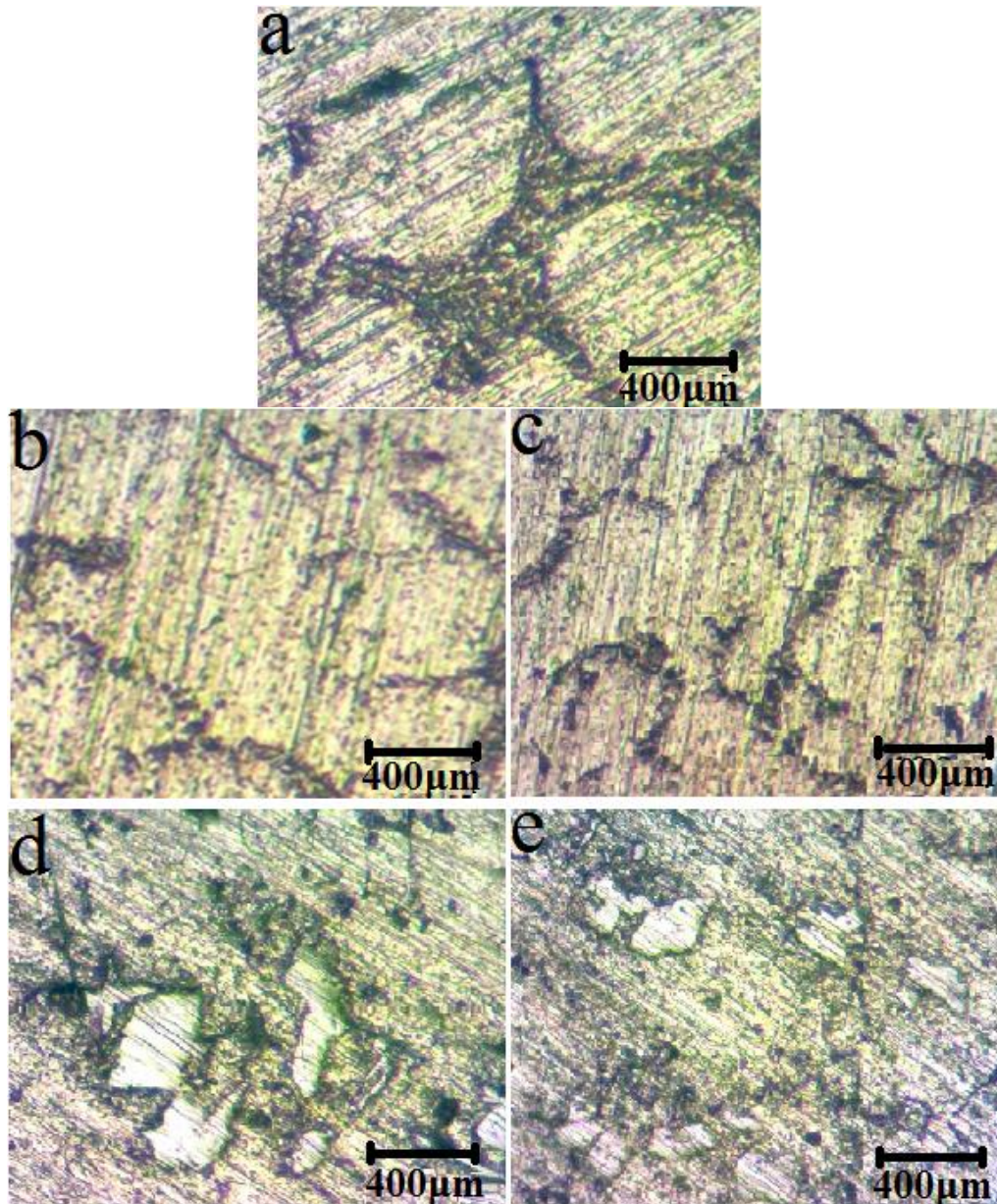
**Fig. 6. OPM of (a) Unheat treated Al-Mg-Si-0%Cr (b) Unheat treated Al-Mg-Si-1.0%Cr (c) Heat treated Al-Mg-Si-1.0%Cr (d) Unheat treated Al-Mg-Si-1.5%Cr (e) heat treated Al-Mg-Si-1.5%Cr alloy samples**

could be ascribed to the appropriate volume concentration of chromium in the grain boundary, which limits grain growth [69]. This is an attestation to the affirmation of the grain refinement ability of Cr particles reported by several authors [70-72]. Moreover, as it can be seen in Fig. 7a, Al-Mg-Si-0%Cr alloy sample exhibited different degrees of micro porosities, cleavages, void and numerous dimples. However, these defects were minimal in the un-heat treated Al-Mg-Si-1.0%Cr alloy sample, and reduction in defect became more glaring after

heat treatment. The reduced defect characteristic displaced by this alloy could as well be traceable to the effect of chromium, which perhaps reduces the entrapment of gases during casting [73-75]. It is also worthy of note that the active re-crystallization in Al-Mg-Si-0%Cr resulted in the formation of brand-new grains in the prior grain boundaries. However, the recrystallization level reduces with the inclusion of chromium, which acted as a barrier to the grain boundary's migration [74,76].
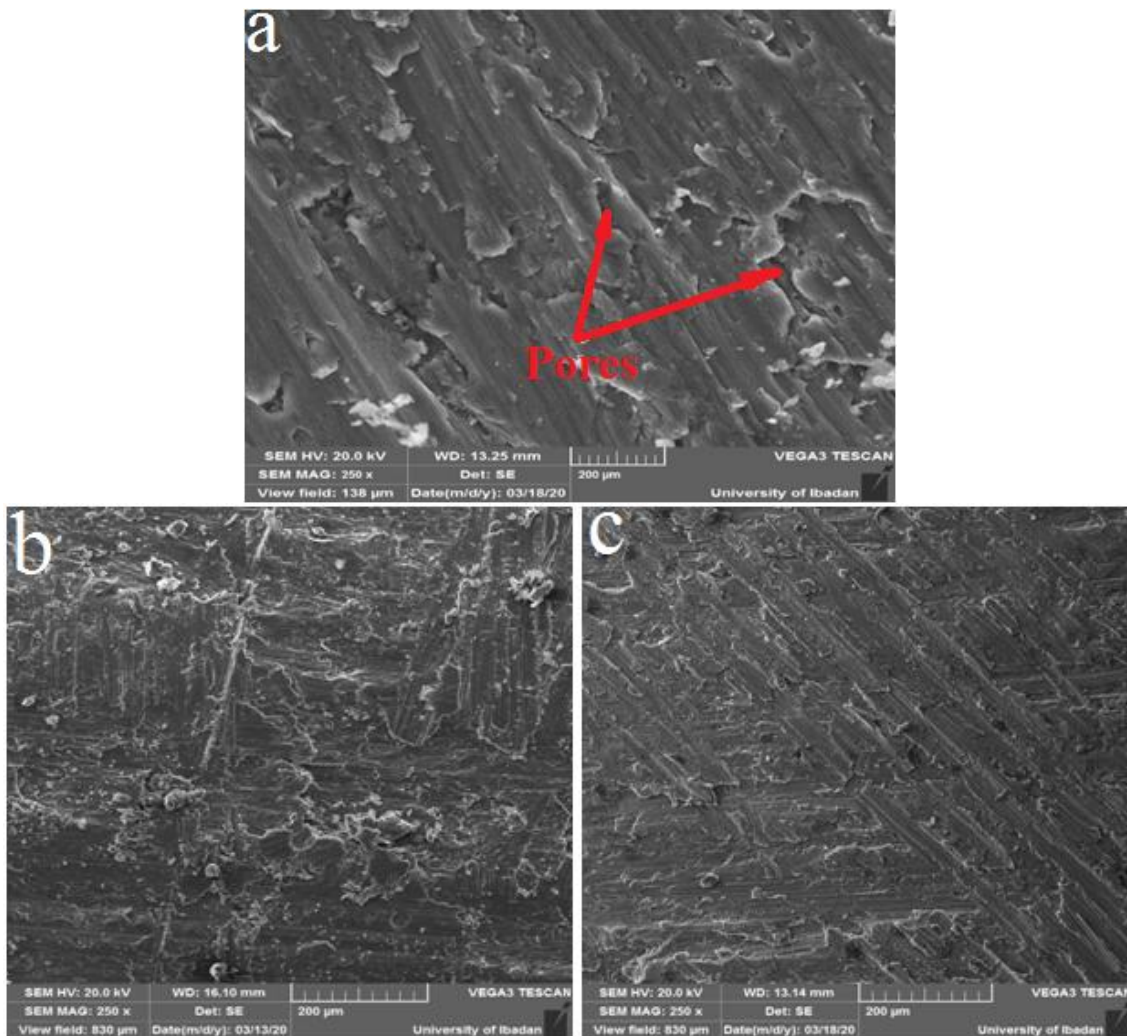
**Fig. 7. SEM of (a) Unheat treated Al-Mg-Si-0%Cr (b) Unheat treated Al-Mg-Si-1.0%Cr  (c) Heat treated Al-Mg-Si-1.0%Cr samples**

## 4. CONCLUSIONS

The effects of the inclusion of chromium in Al-Mg-Si alloy and subsequent heat treatment on the behavioural response of Al-Mg-Si-Cr were investigated. The corrosion, hardness, impact strength, tensile strength, and microstructural properties of un-heat treated and heat treated Al-Mg-Si-Cr alloys were examined based on established procedures. The following conclusions were drawn from the experimental results:

(a) Heat treated Al-Mg-Si-1.0%Cr alloy sample exhibited the highest tensile strength and lowest corrosion rate of 152 MPa and 0.0014 mm/year, respectively.

(b) The inclusion of Cr particles in Al-Mg-Si alloy sample increased hardness from 35.03 Kgf/mm$^2$ (hardness of Al-Mg-Si-0%Cr alloy sample) to a maximum value of 126.54 Kgf/mm$^2$ (hardness of Al-Mg-Si-1.5%Cr alloy sample). After heat treatment, the hardness of Al-Mg-Si-0%Cr alloy sample increased to 80.84 Kgf/mm$^2$, while that of Al-Mg-Si-1.5%Cr alloy sample decreased slightly to 120.88 Kgf/mm$^2$.

(c) Chromium particles inclusion in Al-Mg-Si alloy sample increased impact strength from 9.52 J/mm$^2$ (impact strength of Al-Mg-Si-0%Cr alloy sample) to a maximum value of 19.04 J/mm$^2$ (impact strength of Al-Mg-Si-2.0%Cr alloy sample). After heat treatment, the impact strength of Al-Mg-Si-0%Cr alloy sample increased slightly to 10.09 J/mm$^2$, while that of Al-Mg-Si-2.0%Cr alloy sample decreased slightly to 17.57 J/mm$^2$.

(d) Inclusion of Cr particles in Al-Mg-Si alloy improved its surface morphology. Al-Mg-Si-

1.0%Cr alloy sample was adjudged as the best alloy that possesses refined microstructural characteristics when compared to other Al-Mg-Si alloys with Cr content. Therefore, this sample is recommended as a potential material for machine tools and other structural applications.

## FUNDING

The funding of this research was done by the authors.

## AVAILABILITY OF DATA AND MATERIAL

The authors declare that the data and list of materials used for this research are included in the manuscript.

## CODE AVAILABILITY

The corrosion analysis was conducted using NOVA 2.1.2 software.

## COMPETING INTERESTS

The authors declare that there is no conflict of interest and known competing financial interests or personal relationships that could have appeared to influence the work reported in this manuscript.

## REFERENCES

1. Zhang X, Chen Y, Hu J. Recent advances in the development of aerospace materials. Progress in Aerospace Sciences. 2018;97:22-34.
2. Hung FS. Design of lightweight aluminum alloy building materials for corrosion and wear resistance. Emerging Materials Research. 2020;9(3):750-757.
3. Musfirah AH, Jaharah AG. Magnesium and aluminum alloys in automotive industry. Journal of Applied Sciences Research. 2012;8(9):4865-4875.
4. Jeong C, Leem J, Sheppard K, Choi CH. Air-impregnated nanoporous anodic aluminum oxide layers for enhancing the corrosion resistance of aluminum. Langmuir. 2015;31(40):11040-11050.
5. Barthwal S, Lim SH. Robust and chemically stable superhydrophobic aluminum-alloy surface with enhanced corrosion resistan-ceproperties. International Journal of Precision Engineering and Manufacturing-Green Technology. 2020;7(2):481-492.
6. Vengatesh P, Kulandainathan MA. Hierarchically ordered self-lubricating superhydrophobic anodized aluminum surfaces with enhanced corrosion resistance. ACS Applied Materials and Interfaces. 2015;7(3):1516-1526.
7. Tecchio P, McAlister C, Mathieux F, Ardente F. In search of standards to support circularity in product policies: A systematic approach. Journal of Cleaner Production. 2017;168:1533-1546.
8. Ghosh P, Yusop MZ, Satoh S, Subramanian M, Hayashi A, Hayashi Y, Tanemura M. Transparent and flexible field electron emitters based on the conical nanocarbon structures. Journal of the American Chemical Society. 2010;132(12):4034-4035.
9. Bhowmik A, Mishra D. A comprehensive study of an aluminum alloy AL-5052. Advance Physics Letter. 2016; 3(1):20-22.
10. Huang K, Marthinsen K, Zhao Q, Loge RE. The double-edge effect of second-phase particles on the recrystallization behaviour and associated mechanical properties of metallic materials. Progress in Materials Science. 2018;92:284-359.
11. Li XP, Wang XJ, Saunders M, Suvorova A, Zhang LC, Liu YJ, Sercombe TB. A selective laser melting and solution heat treatment refined Al–12Si alloy with a controllable ultrafine eutectic microstructure and 25% tensile ductility. Acta Materialia. 2015;95:74-82.
12. Zhang XY, Fang G, Leeflang S, Böttger AJ, Zadpoor AA, Zhou J. Effect of subtransus heat treatment on the microstructure and mechanical properties of additively manufactured Ti-6Al-4V alloy. Journal of Alloys and Compounds. 2018;735:1562-1575.
13. Santhosh R, Geetha M, Rao MN. Recent developments in heat treatment of beta titanium alloys for aerospace applications. Transactions of the Indian Institute of Metals. 2017;70(7):1681-1688.
14. Safarbali B, Shamanian M, Eslami A. Effect of post-weld heat treatment on joint properties of dissimilar friction stir welded 2024-T4 and 7075-T6 aluminum alloys. Transactions of Nonferrous Metals Society of China. 2018;28(7):1287-1297.

15. Mohamed AMA, Samuel FH. A review on the heat treatment of Al-Si-Cu/Mg casting alloys. Heat Treatment-Conventional and Novel Applications. 2012;55-72.

16. Liu P, Hu JY, Li HX, Sun SY, Zhang YB. Effect of heat treatment on microstructure, hardness and corrosion resistance of 7075 Al alloys fabricated by SLM. Journal of Manufacturing Processes. 2020;60: 578-585.

17. Jin S, Ngai T, Zhang G, Zhai T, Jia S, Li L. Precipitation strengthening mechanisms during natural ageing and subsequent artificial aging in an Al-Mg-Si-Cu alloy. Materials Science and Engineering: A. 2018;724:53-59.

18. Ma P, Zhan L, Liu C, Wang Q, Li H, Liu D, Hu Z. Pre-strain-dependent natural ageing and its effect on subsequent artificial ageing of an Al-Cu-Li alloy. Journal of Alloys and Compounds. 2019;790:8-19.

19. Engler O, Marioara CD, Aruga Y, Kozuka M, Myhr OR. Effect of natural ageing or pre-ageing on the evolution of precipitate structure and strength during age hardening of Al–Mg–Si alloy AA 6016. Materials Science and Engineering: A. 2019;759:520-529.

20. Prach O, Trudonoshyn O, Randelzhofer P, Körner C, Durst K. Effect of Zr, Cr and Sc on the Al–Mg–Si–Mn high-pressure die casting alloys. Materials Science and Engineering: A. 2019;759:603-612.

21. Li GJ, Guo MX, Wang Y, Zheng CH, Zhang JS, Zhuang LZ. Effect of Ni addition on microstructure and mechanical properties of Al–Mg–Si–Cu–Zn alloys with a high Mg/Si ratio. International Journal of Minerals, Metallurgy, and Materials. 2019;26(6):740-751.

22. Lv Z, Fu H, Xing J, Ma S, Hu Y. Microstructure and crystallography of borides and mechanical properties of Fe–B–C–Cr–Al alloys. Journal of Alloys and Compounds. 2016;662:54-62.

23. Ding L, Jia Z, Liu Y, Weng Y, Liu Q. The influence of Cu addition and pre-straining on the natural aging and bake hardening response of Al-Mg-Si alloys. Journal of Alloys and Compounds. 2016;688: 362-367.

24. Weng Y, Jia Z, Ding L, Muraishi S, Liu Q. Clustering behavior during natural aging and artificial aging in Al-Mg-Si alloys with different Ag and Cu addition. Materials Science and Engineering:A. 2018;732: 273-283.

25. Li C, Liu K, Chen XG. Improvement of elevated-temperature strength and recrystallization resistance via Mn-containing dispersoid strengthening in Al-Mg-Si 6082 alloys. Journal of Materials Science and Technology. 2020;39: 135-143.

26. Lu G, Nie S, Wang J, Zhang Y, Wu T, Liu Y, Liu C. Enhancing the bake-hardening responses of a pre-aged Al-Mg-Si alloy by trace Sn additions. Journal of Materials Science and Technology. 2020;40:107-112.

27. Odoh D, Mahmoodkhani Y, Wells M. Effect of alloy composition on hot deformation behavior of some Al-Mg-Si alloys. Vacuum. 2018;149:248-255.

28. Vilamosa V, Clausen AH, Borvik T, Skjervold SR, Hopperstad OS. Behaviour of Al-Mg-Si alloys at a wide range of temperatures and strain rates. International Journal of Impact Engineering. 2015;86:223-239.

29. Mikhailovskaya AV, Golovin IS, Zaitseva AA, Portnoi VK, Drottboom P, Cifre J. Effect of Mn and Cr additions on kinetics of recrystallization and parameters of grain-boundary relaxation of Al-4.9 Mg alloy. The Physics of Metals and Metallography. 2013;114(3):246-255.

30. Assaad A. Quench sensitivity of 6xxx aluminum alloys (Master's thesis, University of Waterloo);2016.

31. Zuo J, Hou L, Shi J, Cui H, Zhuang L, Zhang J. The mechanism of grain refinement and plasticity enhancement by an improved thermomechanical treatment of 7055 Al alloy. Materials Science and Engineering: A. 2017;702:42-52.

32. Kim B, Park CH, Kim HS, You BS, Park SS. Grain refinement and improved tensile properties of Mg–3Al–1Zn alloy processed by low-temperature indirect extrusion. Scripta Materialia. 2014;76: 21-24.

33. Ertug B, Kumruoglu LC. 5083 type Al-Mg and 6082 type Al-Mg-Si alloys for ship building. American Journal of Engineering Research. 2015;146-150.

34. Ji S, Watson D, Fan Z, White M. Development of a super ductile diecast Al–Mg–Si alloy. Materials Science and Engineering: A. 2012;556:824-833.

35. Fan XB, He ZB, Zhou WX, Yuan SJ. Formability and strengthening mechanism of solution treated Al–Mg–Si alloy sheet under hot stamping conditions. Journal of

Materials Processing Technology. 2016; 228:179-185.

36. Man J, Jing L, Jie SG. The effects of Cu addition on the microstructure and thermal stability of an Al–Mg–Si alloy. Journal of Alloys and Compounds. 2007;437(1-2):146-150.

37. Sarraf M, Nasiri-Tabrizi B, Dabbagh A, Basirun WJ, Sukiman NL. Optimized nanoporous alumina coating on AA3003-H14 aluminum alloy with enhanced tribo-corrosion performance in palm oil. Ceramics International. 2020;46(6):7306-7323.

38. McCafferty E. Validation of corrosion rates measured by the Tafel extrapolation method. Corrosion Science. 2005;47(12):3202-3215.

39. Awe AA, Adedayo SM, Olabamiji TS. Design, development and performance evaluation of A 5-Ton capacity brinell hardness testing machine. Journal of Physics: Conference Series. 2019;1378(3):1-12.

40. Dutta A, Saha SK, Adhikari U, Banerjee P, Sukul D. Effect of substitution on corrosion inhibition properties of 2-(substituted phenyl) benzimidazole derivatives on mild steel in 1 M HCl solution: A combined experimental and theoretical approach. Corrosion Science. 2017;123: 256-266.

41. Fayomi OSI, Akande IG, Oluwole OO, Daramola D. Effect of water-soluble chitosan on the electrochemical corrosion behaviour of mild steel. Chemical Data Collections. 2018;17:321-326.

42. Lgaz H, Bhat KS, Salghi R, Jodeh S, Algarra M, Hammouti B, Essamri A. Insights into corrosion inhibition behavior of three chalcone derivatives for mild steel in hydrochloric acid solution. Journal of Molecular Liquids. 2017;238:71-83.

43. Abd-El-Nabey B.A, Goher YM, Fetouh HA, Karam MS. Anticorrosive properties of chitosan for the acid corrosion of aluminium. Portugaliae Electrochimica Acta. 2015;33(4):231-239.

44. Akande IG, Oluwole OO, Fayomi OSI. Optimizing the defensive characteristics of mild steel via the electrodeposition of ZnSi$_3$-N$_4$ reinforcing particles. Defence Technology. 2019;15(4):526-532.

45. Gupta RK, Malviya M, Verma C, Quraishi MA. Aminoazobenzene and diaminoazobenzene functionalized graphene oxides as novel class of corrosion inhibitors for mild steel: experimental and DFT studies. Materials Chemistry and Physics. 2017;198:360-373.

46. Akande IG, Fayomi OSI, Oluwole OO. Anticorrosion potential of inhibitive suphtrim drug on aluminium alloys in 0.5 M H$_2$SO$_4$. Journal of Bio-and Tribo-Corrosion. 2020;6(4):1-8.

47. Mirzakhani B, Payandeh Y. Combination of sever plastic deformation and precipitation hardening processes affecting the mechanical properties in Al–Mg–Si alloy. Materials and Design. 2015;68: 127-133.

48. Ashjari M, Feizi AJ. 7xxx aluminum alloys; strengthening mechanisms and heat treatment: a review. Material Sci and Eng Int J. 2018;2(2):49-53.

49. Pedrazzini S, Galano M, Audebert F, Collins DM, Hofmann F, Abbey B, Smith GDW. Strengthening mechanisms in an Al-Fe-Cr-Ti nano-quasicrystalline alloy and composites. Materials Science and Engineering: A. 2016;672:175-183.

50. Lodgaard L, Ryum N. Precipitation of dispersoids containing Mn and/or Cr in Al–Mg–Si alloys. Materials Science and Engineering: A. 2000;283(1-2):144-152.

51. Gül C, Çömez N, Çivi C, Durmuş H. Reliability analysis of brinell hardness results for aged alumix321/SiC composites. Transactions of the Indian Institute of Metals. 2019; 72(9): 2311-2318.

52. Wang AQ, Guo HD, Han, HH, Xie JP. Effect of solid solution and ageing treatments on the microstructure and mechanical properties of the SiCp/Al-Si-Cu-Mg Composite. Kemija u Industriji. 2017;66(7-8):345−351.

53. Aboulkhair NT, Maskery I, Tuck C, Ashcroft I, Everitt NM. The microstructure and mechanical properties of selectively laser melted AlSi10Mg: The effect of a conventional T6-like heat treatment. Materials Science and Engineering: A. 2016;667: 139-146.

54. Read N, Wang W, Essa K, Attallah MM. Selective laser melting of AlSi10Mg alloy: Process optimisation and mechanical properties development. Materials and Design (1980-2015). 2015;65:417-424.

55. Mozammil S, Karloopia J, Verma R, Jha PK. Effect of varying TiB2 reinforcement and its ageing behaviour on tensile and hardness properties of in-situ Al-4.5% Cu-xTiB$_2$ composite. Journal of Alloys and Compounds. 2019;793:454-466.

56. Herrera-Ramírez LC, Castell P, Castillo-Rodríguez M, Fernández Á, Guzman de Villoria R. The effect of a semi-industrial masterbatch process on the carbon nanotube agglomerates and its influence in the properties of thermoplastic carbon nanotube composites. Journal of Polymer Science Part B: Polymer Physics. 2017;55(2):189-197.

57. Wang PH, Sarkar S, Gulgunje P, Verghese N, Kumar S. Fracture mechanism of high impact strength polypropylene containing carbon nanotubes. Polymer. 2018;151:287-298.

58. Zhang H, Zhang Z. Impact behaviour of polypropylene filled with multi-walled carbon nanotubes. European Polymer Journal. 2007;43(8):3197-3207.

59. Rashed HM. Control of distortion in aluminium heat treatment. Fundamentals of Aluminium Metallurgy. Woodhead Publishing. 2018;495-524.

60. Ajide OO, Ogochukwu CD, Akande IG, Petinrin MO, Ismail OS, Oluwole OO, Oyewola OM. Production and characterisation of Al-Mg-Cr alloy for machine tool applications, Test Engineering and management. 2020;83:1-9.

61. Reddy AC, Zitoun E. Tensile properties and fracture behavior of 6061/Al2O3 metal matrix composites fabricated by low pressure die casting process. International Journal of Materials Sciences. 2011; 6(2):147-157.

62. Prabu SB, Karunamoorthy L, Kathiresan S, Mohan B. Influence of stirring speed and stirring time on distribution of particles in cast metal matrix composite. Journal of Materials Processing Technology. 2006; 171(2):268-273.

63. Balasubramanian I, Maheswaran R. Effect of inclusion of SiC particulates on the mechanical resistance behaviour of stir-cast AA6063/SiC composites. Materials and Design (1980-2015). 2015;65: 511-520.

64. Li W, Li S, Liu J, Zhang A, Zhou Y, Wei Q, Shi Y. Effect of heat treatment on AlSi10Mg alloy fabricated by selective laser melting: Microstructure evolution, mechanical properties and fracture mechanism. Materials Science and Engineering: A. 2016;663: 116-125.

65. Tian W, Li, Wang B, Liu J, Yu M. Pitting corrosion of naturally aged AA 7075 aluminum alloys with bimodal grain size. Corrosion Science. 2016;113:1-16.

66. Luo C, Albu SP, Zhou X, Sun Z, Zhang X, Tang Z, Thompson GE. Continuous and discontinuous localized corrosion of a 2xxx aluminium–copper–lithium alloy in sodium chloride solution. Journal of Alloys and Compounds. 2016;658:61-70.

67. Hafenstein S, Werner E. Pressure dependence of age-hardenability of aluminum cast alloys and coarsening of precipitates during hot isostatic pressing. Materials Science and Engineering: A. 2019;757:62-69.

68. Ajide OO, Otesile AO, Salau TAO, Ismail OS, Oyewola OM. Investigating effect of zinc content on the mechanical and corrosion responses of Al6063-SiC composite. Current Journal of Applied Science and Technology. 2017;22(3):1-10.

69. Ezatpour HR, Sajjadi SA, Sabzevar MH, Huang Y. Investigation of microstructure and mechanical properties of Al6061-nanocomposite fabricated by stir casting. Materials and Design. 2014;55:921-928.

70. Bermingham MJ, StJohn DH, Krynen J, Tedman-Jones S, Dargusch MS. Promoting the columnar to equiaxed transition and grain refinement of titanium alloys during additive manufacturing. Acta Materialia. 2019;168:261-274.

71. Lv J, Guo W, Liang T, Yang M. The effects of ball milling time and surface enriched chromium on microstructures and corrosion resistance of AISI 304 stainless steel. Materials Chemistry and Physics. 2017;197:79-86.

72. Fattah-Alhosseini A, Vafaeian S. Influence of grain refinement on the electrochemical behavior of AISI 430 ferritic stainless steel in an alkaline solution. Applied Surface Science. 2016;360:921-928.

73. Alizadeh A, Taheri-Nassaj E, Hajizamani M. Hot extrusion process effect on mechanical behavior of stir cast Al based composites reinforced with mechanically milled B4C nanoparticles. Journal of Materials Science and Technology. 2011;27(12):1113-1119.

74. Fayomi OSI, Joseph OO, Akande IG, Ohiri CK, Enechi KO, Udoye NE. Effect of CCBP doping on the multifunctional Al-0.5 Mg-15CCBP superalloy using liquid metallurgy process for advanced application. Journal of Alloys and Compounds. 2019;783:246-255.

75. Akbari MK, Mirzaee O, Baharvandi HR. Fabrication and study on mechanical properties and fracture behavior of nanometric $Al_2O_3$ particle-reinforced A356 composites focusing on the parameters of vortex method. Materials & Design. 2013; 46:199-205.

76. Zhou X, Fu R, Fu D, Wang Y. Ultrasound frequency-dependent microstructures of electrodeposited Ni nanocrystals for modifying mechanical properties. Journal of Materials Science. 2020;55(30): 14980-15004.

---

*Peer-review history:*
*The peer review history for this paper can be accessed here:*
*https://www.sdiarticle5.com/review-history/102261*

---